Structural Chemistry and Electronic Properties of the $n = 3$ Ruddlesden−Popper Phases $Ca_4Mn_2FeO_{9.75}$ and $Sr_4Mn_2FeO_{9.80}$

P. D. Battle,*,† W. R. Branford,† A. Mihut,‡ M. J. Rosseinsky,*,† J. Singleton,‡ J. Sloan,†,§ L. E. Spring,†,‡ and J. F. Vente†

Inorganic Chemistry Laboratory, Department of Chemistry, University of Oxford, South Parks Road, Oxford, OX1 3QR, UK, Clarendon Laboratory, Department of Physics, University of Oxford, Parks Road, Oxford, OX1 3PU, UK, and Department of Materials, University of Oxford, Parks Road, Oxford, OX1 3PH, UK

Received July 27, 1998

The room-temperature crystal structures of the $n = 3$ Ruddlesden−Popper phases $Ca_4Mn_2FeO_{9.75}$ and $Sr_4Mn_2FeO_{9.80}$ have been refined from neutron and X-ray powder diffraction data. Both adopt space group $I4/mmm$ with (a,c) = (Ca, 3.73683(1), 27.0860(1) Å), (Sr, 3.83393(1), 27.8148(1) Å). In both compounds the cation site at the center of the perovskite blocks is preferentially occupied by Fe (Ca, Mn:Fe = 0.424:0.576(4)), and the anion vacancies are found around this site. The occupied anion sites show static disorder in $Ca_4Mn_2FeO_{9.75}$ but not in $Sr_4Mn_2FeO_{9.80}$. Both compounds are electrical insulators which order antiferromagnetically at $T_N = 75$ K (Ca) or 90 K (Sr). Susceptibility and $M(H)$ data suggest that not all the Mn and Fe cations take part in the long-range magnetic ordering, and there is evidence of a spin glass transition in both compounds at ∼11 K. The magnetic structure of $Ca_4Mn_2FeO_{9.75}$ at 5 K has been determined by neutron diffraction. No ordered moment was detected on the Mn/Fe site at the center of the perovskite blocks; 0.74(1) μ_B per transition metal cation was measured at the sites on the block edges. Possible causes of magnetic frustration in this crystal structure are considered. $Ca_4Mn_2FeO_{9.75}$ has a magnetotresistance of −4% at 137 K in a 14 T field.

Introduction

The magnetotransport properties of Mn-containing oxides have stimulated a great deal of research activity in recent years.[1,2] The majority of the compounds of interest show a spontaneous magnetization at low temperatures and contain mixed-valence Mn^{3+}/Mn^{4+} cations in a perovskite-related crystal structure. It has been demonstrated that, in many cases, their resistivity at temperatures slightly above the Curie temperature (T_c) drops by several orders of magnitude on the application of a magnetic field. No adequate explanation of this colossal magnetoresistance (CMR; $(\rho_B - \rho_0)/\rho_0 \sim -0.99$) behavior is presently available, although it is generally agreed that double exchange[3] on the Mn sublattice is an important factor. However, models which rely on this mechanism cannot explain the observation[4] of CMR in the pyrochlore $Tl_2Mn_2O_7$, which, as an oxide of Mn^{4+}, does not have a nonintegral number of electrons per Mn, as is required if the double exchange mechanism is to operate. The range of perovskite-related compounds which show the effect is not limited to those with a formula of the type ABO_3. It also includes[5,6] compounds having the formula $A_2A'B_2O_7$, that is, the $n = 2$ members of the Ruddlesden−Popper (RP) family[7] $(A,A')_{n+1}B_nO_{3n+1}$, of which perovskite ABO_3 is the $n = \infty$ end member. All the members of this family can be considered to consist of blocks of perovskite-like, corner-sharing BO_6 octahedra which extend to infinity in the xy plane and are n octahedra thick parallel to z; neighboring blocks are separated by rock salt layers, so that the formula can usefully be written as $((A,A')BO_3)_n(A,A')O$. We recently reported[8] the crystal structure and magnetic properties of an $n = 3$ compound $Ca_4Mn_3O_{10}$. This material shows an orthorhombic distortion of the tetragonal structure usually associated with RP phases, and it consequently orders as a weak ferromagnet at 115 K. However, despite the presence of a spontaneous magnetization, magnetotransport measurements[9] revealed a level of magnetoresistance in this compound which, although significant ($\rho_B - \rho_0/\rho_0 \sim -0.4$, $B = 14$ T, $T = 5$K), was not as high as that seen in $n = 2$ phases.

† Inorganic Chemistry Laboratory, Department of Chemistry.
‡ Clarendon Laboratory, Department of Physics.
§ Department of Materials.

(1) Kusters, R. M.; Singleton, J.; Keen, D. A.; McGreevy, R.; Hayes, W. *Physica* 1989, *B155*, 363.
(2) Ramirez, A. P. *J. Phys.: Condens. Matter* **1997**, *9*, 8171.
(3) Zener, C. *Phys. Rev.* **1951**, *82*, 403.
(4) Shimakawa, Y.; Kubo, Y.; Manako, T. *Nature* **1996**, *379*, 53.
(5) Battle, P. D.; Blundell, S. J.; Green, M. A.; Hayes, W.; Honold, M.; K. Klehe, A.; Laskey, N. S.; Millburn, J. E.; Murphy, L.; Rosseinsky, M. J.; Samarin, N. A.; Singleton, J.; Sluchanko, N. A.; Sullivan, S. P.; Vente, J. F. *J. Phys.: Condensed Matter* **1996**, *8*, L427.
(6) Moritomo, Y.; Asamitsu, A.; Kuwahara, H.; Tokura, Y. *Nature* **1996**, *380*, 141.
(7) Ruddlesden, S. N.; Popper, P. *Acta Crystallogr.* **1958**, *11*, 541.
(8) Battle, P. D.; Green, M. A.; Lago, J.; Millburn, J. E.; Rosseinsky, M. J.; Vente, J. F. *Chem. Mater.* **1998**, *10*, 658.
(9) Mihut, A. I.; Spring, L. E.; Bewley, R. I.; Blundell, S. J.; Hayes, W.; Jestädt, Th.; Lovett, B. W.; McDonald, R.; Pratt, F. L.; Singleton, J.; Battle, P. D.; Lago, J.; Rosseinsky, M. J.; Vente, J. F. *J. Phys.: Condensed Matter* **1998**, *10*, L727.

10.1021/cm9807384 CCC: $18.00
Published on Web 02/25/1999

We have now prepared the compounds $Ca_4Mn_2FeO_{10-\delta}$ and $Sr_4Mn_2FeO_{10-\delta}$ in order to ascertain whether the structural and electronic changes induced by the introduction of Fe and Sr can have a beneficial effect on the magnetotransport properties of the $n = 3$ phases. The introduction of Fe^{4+} into an oxide of Mn^{4+} would lead to the presence of both d^4 and d^3 cations, as is the case in the Mn^{3+}/Mn^{4+} oxides which show CMR. Furthermore, the replacement of Ca^{2+} by the more basic Sr^{2+} would be expected to lead to a broadening of the bands derived principally from the cation d orbitals and hence to a shift toward itinerant electron behavior. However, the electronic properties of mixed metal oxides are sufficiently complex that, although rational strategies can be devised, nature will often introduce additional complexities. This was demonstrated when Gundakaram et al[10] attempted to create a d^3/d^4 cation mixture by Cr^{3+} doping in the $n = \infty$ RP phase $LnMn^{3+}{}_{1-x}Cr^{3+}{}_xO_3$. Although they were able to preserve ferromagnetic coupling, they did not observe the CMR behavior associated with perovskites in which the d^3/d^4 mix stems from the presence of mixed-valence Mn^{3+}/Mn^{4+}. We describe below the structural and electronic properties of the two new phases $Ca_4Mn_2FeO_{10-\delta}$ and $Sr_4Mn_2FeO_{10-\delta}$ and show that, in this case, the simplistic model is frustrated by the effects of both Mn/Fe and anion disorder, together with incomplete cation oxidation.

Experimental Section

Polycrystalline samples of nominal composition $Ca_4Mn_2FeO_{10-\delta}$ and $Sr_4Mn_2FeO_{10-\delta}$ were prepared by reacting well-ground stoichiometric mixtures of $SrCO_3$, $CaCO_3$, MnO_2, and Fe_2O_3 in air. Both reaction mixtures were heated for 1 day at 800 °C, 1 day at 1000 °C, and 3 days at 1200 °C; the Sr-containing sample only was then heated for 5 days at 1300 °C, 7 days at 1320 °C, and 1 day at 1330 °C. The progress of the reactions was monitored by X-ray powder diffraction, and data were collected on the final products using a Siemens D5000 diffractometer operating with Cu $K_{\alpha 1}$ radiation in Bragg−Brentano geometry. Data were collected over the angular range $10° \le 2\theta \le 120°$, with a step size of $\Delta 2\theta = 0.02°$. The oxygen stoichiometry of the products was determined by dissolving ~30 mg of sample in concentrated hydrochloric acid, purged by a flow of nitrogen gas, in the presence of excess potassium iodide before titrating against sodium thiosulfate solution. Neutron diffraction data covering the *d* spacing range $0.72 \text{ Å} \le d \le 2.38 \text{ Å}$ were collected at room temperature on both $Ca_4Mn_2FeO_{10-\delta}$ and $Sr_4Mn_2FeO_{10-\delta}$ using the backscattering detector bank on the HRPD diffractometer at the ISIS facility, Rutherford Laboratory. In the case of $Ca_4Mn_2FeO_{10-\delta}$, data were also collected at 5 K, and a further data set covering the *d* spacing range $2.13 \text{ Å} \le d \le 5.27 \text{ Å}$ was collected at 5 K on the diffractometer IRIS. Analysis of these data was carried out by the Rietveld method,[11] as implemented in the GSAS program package.[12] $Ca_4Mn_2FeO_{10-\delta}$ was also studied using a JEOL 4000EX high-resolution transmission electron microscope, operated at 400 kV (point resolution = 1.6 Å). Finely ground specimens were dispersed in chloroform in an ultrasonic bath and then placed, dropwise, onto lacy carbon-coated copper grids (Agar 200 mesh). Lattice images were recorded under optimum Scherzer defocus conditions from crystal fragments with their [010] zone axes aligned parallel to the electron beam. Image simulations were calculated using the multislice program in the EMS program package.[13] The magnetic susceptibilities of samples of $Ca_4Mn_2FeO_{10-\delta}$ and $Sr_4Mn_2FeO_{10-\delta}$ contained in gelatin capsules were measured in the temperature range $5 \text{ K} \le T \le 300 \text{ K}$ using a Quantum Design MPMS SQUID magnetometer. Data were collected after cooling both in the absence (ZFC) of an applied field and in the measuring field (FC). Measurements were made in fields of 100 and 1000 G. Hysteresis loops were recorded for $-2000 \text{ G} \le H \le 2000 \text{ G}$ at selected temperatures after cooling the samples in a field of 2000 G. Magnetoresistance measurements were carried out on a sintered bar (approximately $2 \times 2 \times 5$ mm^3) of $Ca_4Mn_2FeO_{10-\delta}$ using a dc four-terminal method with the current (<50 μA) perpendicular to the applied magnetic field. Electrical contacts to the bar were made with silver epoxy to evaporated gold pads. The zero-field resistivity was measured as a function of temperature in the range $130 \text{ K} \le T \le 285 \text{ K}$ (below 130 K the signal became immeasurably large). Resistivity was then measured as a function of field ($0 \text{ T} < B < 14 \text{ T}$) at constant temperatures of 137 and 188 K.

Results

Although more forcing conditions were needed to prepare the Sr-containing compound, the X-ray diffraction patterns of our final products were quantitatively consistent with the formation of monophasic $n = 3$ RP samples. Volumetric analysis showed the compositions of the reaction products to be $Ca_4Mn_2FeO_{9.75(5)}$ and $Sr_4Mn_2FeO_{9.80(5)}$. Assuming that Mn is only present in the +4 oxidation state, the mean oxidation states of Fe in the Ca- and Sr-containing compounds are thus 3.5(1) and 3.6(1), respectively. Attempts to analyze the neutron diffraction data collected at room temperature on $Ca_4Mn_2FeO_{9.75}$ using the orthorhombic space group (*Pbca*) adopted by $Ca_4Mn_3O_{10}$ were unsuccessful, and it became clear that the Fe-doped phase has tetragonal symmetry. Structure refinements in *I*4/*mmm* were more successful, provided that the transition metal cations were allowed to order over the crystallographically distinct 6-coordinate sites, with Mn and Fe preferentially occupying the outer and central layers of the perovskite blocks, respectively (Figure 1). Preliminary refinements of the thermal parameters of the oxide ions indicated that the anions in the equatorial (*xy*) plane of the MnO_6 octahedra are displaced significantly from their ideal positions on the {100} mirror planes. The X-ray and neutron diffraction data were searched for superlattice reflections which might have proved that these displacements represent a cooperative rotation of the octahedra about the *z* axis, but no such evidence could be found. We therefore concluded that this part of the oxide sublattice is subject to static disorder and performed our definitive refinements in space group *I*4/*mmm*. The total oxygen content was constrained to the value determined by volumetric analysis, and although the distribution of transition metals over the two available sites was allowed to vary, the Mn:Fe ratio was constrained to be 2:1. The use of anisotropic thermal parameters for the cations did not result in any significant improvement in the overall fit quality. Our final refinements made simultaneous use of the X-ray and neutron data. This approach was adopted because the negative neutron scattering length of Mn results in a low mean scattering length for a site which is partially occupied by both Mn and Fe, and the X-ray data

(10) Gundakaram, R.; Arulraj, A.; Vanitha, P. V.; Rao, C. N. R.; Gayathri, N.; Raychaudhuri, A. K.; Cheetham, A. K. *J. Solid State Chem.* **1996**, *127*, 354.

(11) Rietveld, H. M. *J. Appl. Crystallogr.* **1969**, *2*, 65.

(12) Larson, A. C.; von Dreele, R. B. General Structure Analysis System (GSAS), *Los Alamos National Laboratories*, Report LAUR 86-748, 1990.

(13) Stadelman, P. A. *Ultramicroscopy* **1987**, *21*, 131.

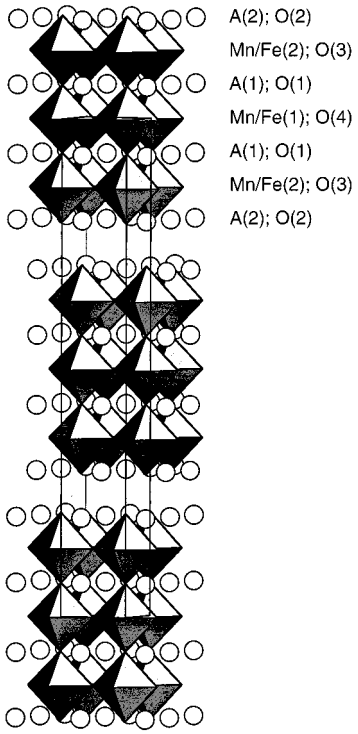

Figure 1. The $n = 3$ Ruddlesden−Popper crystal structure of $Ca_4Mn_2FeO_{9.75}$ and $Sr_4Mn_2FeO_{9.80}$.

effectively serve to locate the 6-coordinate cations. Neutrons are, of course, more sensitive to the disorder on the oxide sublattice. The usual parameters were varied during our structure refinement, but we also included two additional variables to account for the anisotropic peak broadening which was apparent in our neutron data, the peaks with $l \neq 0$ being anomalously broad. The need to use this parameter suggests that the crystallinity of our sample is greater in the *xy* plane than it is along *z*. The structural parameters resulting from these data analysis are listed in Table 1. The displaced oxide ions discussed above are labeled O(3) and O(4). Refinements of site occupancy factors suggested that the anion vacancies occur on the sites O(1) and O(4), which are coordinated to the cation at the center of the perovskite blocks; the thermal parameters lend some support to this conclusion. However, the sensitivity to the defect distribution was low and we cannot confidently rule out other vacancy distributions. The observed and calculated diffraction profiles are shown in Figure 2. The disordered arrangement of O(3) and O(4) around Mn/Fe(2) and Mn/Fe(1), respectively, is depicted in Figure 3, and the consequences for the coordination of Ca(1) and Ca(2) are shown in Figure 4. The bond lengths around the cation sites are listed in Table 2. Our study of $Ca_4Mn_2FeO_{9.75}$ by electron microscopy did not provide any evidence of a supercell, and the diffraction patterns observed (Figure 5) were consistent with our choice of space group $I4/mmm$. However, it is possible that the superlattice would not have been apparent in the zones we observed, and we therefore cannot use these data as proof of our model. The lattice images (Figure 5) recorded from our sample did provide convincing evidence that it has a well-ordered $n = 3$ RP microstructure, with no evidence for the intergrowth of RP phases having different values of *n*, in contrast to the $n = 2$ phases studied previously.[14] There is excellent agreement between the observed image and that calculated from the refined atomic coordinates of $Sr_4Mn_2FeO_{9.80}$ using a defocus of −800 Å and a foil thickness of 14.9 Å.

Simultaneous analysis of X-ray and neutron diffraction data was also used in the refinement of the crystal structure of $Sr_4Mn_2FeO_{9.80}$. The resulting structural model is very similar to that described above for the Ca analogue, but there was evidence of neither positional disorder on the anion sublattice nor anisotropic peak broadening in the Sr compound. The oxygen deficiency was again found to occur on sites O(1) and O(4). The final values of the structural parameters are listed in Table 3 and the corresponding bond lengths and bond angles are presented in Table 4. Figure 6 emphasizes the anisotropic nature of the mean displacements of the oxide ions. The observed and calculated diffraction patterns are drawn in Figure 7.

The temperature dependence of the molar magnetic susceptibility of $Ca_4Mn_2FeO_{9.75}$ is shown in Figure 8, and the corresponding data for $Sr_4Mn_2FeO_{9.80}$ are plotted in Figure 9. The data collected in a field of 1000 G were not significantly different from those illustrated, which were measured in 100 G. The data on the two different compositions are qualitatively similar. The FC susceptibility of both compounds increases with decreasing temperature throughout the measured range, but both show a local maximum, at 75 K in the case of $Ca_4Mn_2FeO_{9.75}$ and at 95 K in the case of $Sr_4Mn_2FeO_{9.80}$. The ZFC and FC data overlie above these maxima, but they diverge at lower temperatures, with the ZFC susceptibility showing a maximum at ∼12 K in both cases. The parameters derived by fitting the high-temperature region (150 K ≤ *T* ≤ 300 K) to a Curie−Weiss Law are listed in Table 5. A molar Curie constant of 7.43 cm^3 K mol^{-1} is predicted by the spin-only formula for a noninteracting mixture of ($2Mn^{4+} + 0.5Fe^{3+} + 0.5Fe^{4+}$) cations. Our initial reaction to the data in Figures 8 and 9 was to hypothesize that the maxima at 75 and 95 K correspond to Néel temperatures (T_N) but that a fraction of the spins are not involved in the long-range antiferromagnetic ordering; these spins subsequently freeze, as in a spin glass, at $T_g \sim 14$ K. The results described below are those of experiments designed to test this hypothesis. When neutron beam time was limited, we chose to focus on the Ca-containing sample. We believe that our magnetization data establish a strong enough similarity in the behavior of these two compounds for it to be reasonable to extrapolate from one to the other, but we shall return to this point below. The central regions of FC $M(H)$ curves recorded on a sample of $Ca_4Mn_2FeO_{9.75}$ are shown in Figure 10, and corresponding data on $Sr_4Mn_2FeO_{9.80}$ are plotted in Figure 11. All the curves recorded in the temperature range 30 K ≤ *T* ≤ 300 K pass through the origin and have a negligible width. This indicates that the samples are antiferromagnetic or paramagnetic at these temperatures; there is no evidence for weak ferromagnetism similar to that observed in $Ca_4Mn_3O_{10}$. However, the $M(H)$ curves measured at 5 K have a finite width and are not symmetrical about

(14) Sloan, J.; Battle, P. D.; Green, M. A.; Rosseinsky, M. J.; Vente, J. F. *J. Solid State Chem.* **1998**, *138*, 135.

Table 1. Structural Parameters of $Ca_4Mn_2FeO_{9.75}$ at Room Temperature[a]

atom	site	fractional occupancy	x	y	z	U_{iso}, U_{eq} (Å^2)	U_{11} (Å^2)	U_{22} (Å^2)	U_{33} (Å^2)
Ca(1)	4e	1	0	0	0.57176(8)	0.0169(5)			
Ca(2)	4e	1	0	0	0.70353(7)	0.0135(5)			
Mn/Fe(1)	2a	0.424/0.576(4)	0	0	0	0.020(1)			
Mn/Fe(2)	4e	0.782/0.212(2)	0	0	0.1400(2)	−0.0006(2)			
O(1)	4e	0.97(1)	0	0	0.06927(8)	0.0367	0.051(1)	0.051(1)	0.008(1)
O(2)	4e	1	0	0	0.21143(6)	0.0182	0.024(1)	0.024(1)	0.005(1)
O(3)	16n	0.5	0	0.562(1)	0.63963(8)	0.0196	0.006(1)	0.018(3)	0.033(1)
O(4)	8j	0.452(5)	0	0.5926(8)	0.5	0.0336	0.010(2)	0.019(4)	0.070(3)

[a] Space group $I4/mmm$; $a = 3.73683(1)$ Å, $c = 27.0860(1)$ Å, $V = 378.227(2)$ Å^3. For all O, $U_{12} = U_{13} = U_{23} = 0$, except for O(3), where $U_{12} = U_{13} = 0$, $U_{23} = -0.001(1)$ Å^2. Agreement indices: neutrons, $R_{wp} = 7.01\%$, $R_p = 5.15\%$, DWd = 0.29; X-rays, $R_{wp} = 5.57\%$, $R_p = 4.39\%$, DWd = 1.78; totals, $R_{wp} = 6.72\%$, $R_p = 4.41\%$, DWd = 0.52. $\chi_{red}^2 = 4.46$ for 68 variables.

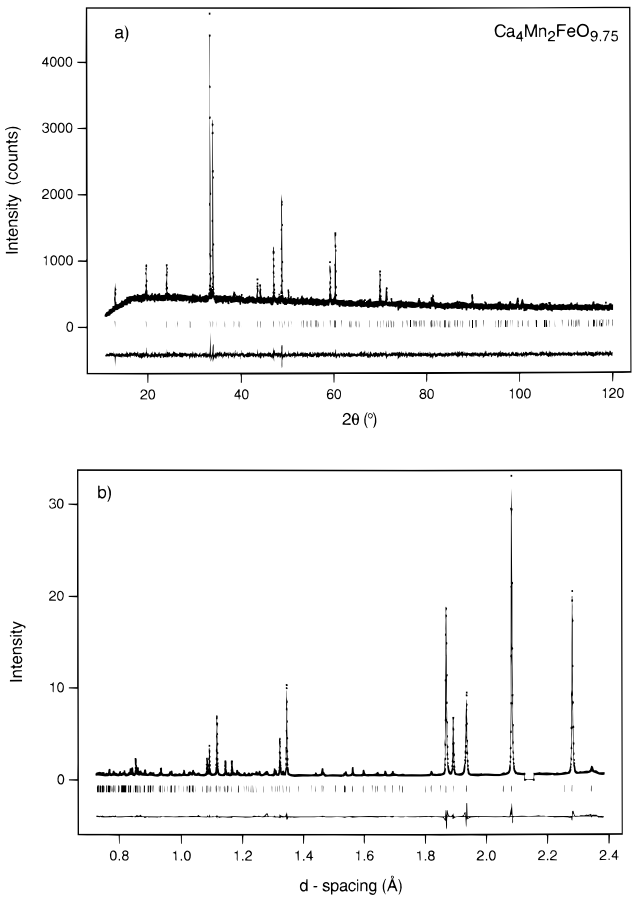

Figure 2. Observed, calculated, and difference (a) X-ray and (b) neutron diffraction profiles of $Ca_4Mn_2FeO_{9.75}$ at room temperature with reflection positions marked. Scattering from the vanadium sample can has been excluded from the neutron data set.

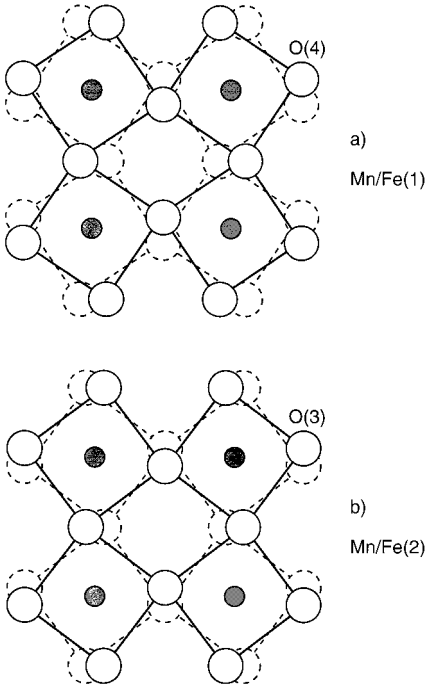

Figure 3. The disordered arrangement of (a) O(4) about Mn/Fe(1) and (b) O(3) about Mn/Fe(2) in the structure of $Ca_4Mn_2FeO_{9.75}$. Solid and dotted circles have the same z coordinate and represent the two disordered configurations.

the origin. This is consistent with there being a spin glass transition in the range 5 K ≤ T ≤ 30 K, as was postulated above on the basis of the susceptibility data.

Neutron diffraction data were collected on $Ca_4Mn_2FeO_{9.75}$ at 5 K using two diffractometers, HRPD and IRIS. The data collected on HRPD (at relatively short d spacings) did not contain any magnetic Bragg peaks and their role was to facilitate refinement of the low-temperature crystal structure. These data were analyzed with the fractional occupancies of all sites fixed at the values determined at room temperature. Furthermore, in view of the absence of low-temperature X-ray data and the resulting poor definition of the variable coordinates of mixed Mn/Fe sites, Mn/Fe(2) was constrained to lie 0.5**c** below the O(3) position. This constraint is consistent with the result of the free refinement used in the analysis of the data collected at room temperature (Table 1). The structural parameters resulting from the refinement of the HRPD 5 K data are presented in Table 6; the bond lengths derived from these parameters do not show any significant difference from those determined at the higher temperature. The data collected on IRIS showed additional Bragg peaks and thus provided clear evidence of long-range antiferromagnetic ordering. Various models for the magnetic structure were tested, and that drawn in Figure 12 gave the best agreement between the observed and calculated intensity distributions; the magnetic unit cell has dimensions $\sqrt{2}a \times \sqrt{2}b \times c$ compared to the chemical unit cell, and the symmetry of the spin structure is orthorhombic rather than tetragonal. This model is related to that used previously to describe $Ca_4Mn_3O_{10}$[8] in that each of the triple-layer perovskite blocks can be thought of as showing G-type antiferromagnetism. However, in the present case the ordered component of the magnetic moment on the central, Fe-rich Mn/Fe(1) sites is zero. Analysis of the IRIS data using this model, with the atomic coordinates fixed at the values deter-

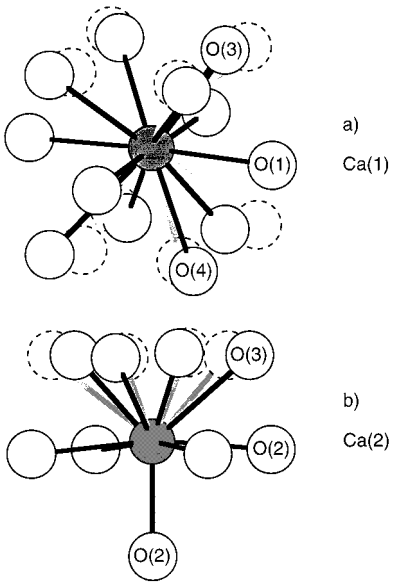

Figure 4. The coordination about (a) Ca(1) and (b) Ca(2) in $Ca_4Mn_2FeO_{9.75}$. Solid and dotted circles represent the two disordered configurations.

mined using the HRPD data, gave a value for the ordered magnetic moment of 0.74(1) μ_B per Mn/Fe(2) site; the moment lies in the *xy* plane, but the direction within the plane cannot be defined from our data. The quality of the fit ($R_{wp} = 4.84\%$; $R_p = 3.76\%$; DWd = 0.37; $\chi_{red}^2 = 1.57$ for 17 variables) can be judged from the diffraction profiles shown in Figure 13. Diffraction patterns collected on warming the sample showed that the magnetic Bragg peaks vanish at 75 K, thus confirming that the local susceptibility maximum reported above does correspond to the Néel temperature.

The resistivity of $Ca_4Mn_2FeO_{9.75}$ in the absence of a magnetic field is plotted as a function of temperature in Figure 14a. The data show a small, activated conductivity ($E_a = 0.15$ eV for 130 K $< T \leq$ 200 K, increasing to 0.21 eV for 200 K $< T \leq$ 285 K) in the measured temperature range (130 K $\leq T \leq$ 285 K); the conductivity below 130 K was too small to be measured using our apparatus. Only a small ($\rho_B - \rho_0/\rho_0 \sim -4\%$) magnetoresistance was observed in fields of up to 14 T at 137 K (Figure 14b). No magnetotransport study was performed on $Sr_4Mn_2FeO_{9.80}$; the magnitude of the zero-field conductivity was comparable to that of the Ca analogue.

Discussion

The results described above demonstrate that it is possible to introduce Fe into the $n = 3$ RP structure of $Ca_4Mn_3O_{10}$. The presence of vacancies on the anion sublattice is unsurprising given the well-documented difficulty[15] of stabilizing Fe^{4+} in an ambient pressure synthesis. The slightly lower degree of reduction to Fe^{3+} in the case of $Sr_4Mn_2FeO_{9.80}$ can be explained in terms of the low acidity of Sr^{2+} compared to that of Ca^{2+}; similar trends have been observed previously in the synthesis of the phases $Sr_2Fe_2O_{5+\delta}$ and $Ca_2Fe_2O_{5+\delta}$.[16] The success of the synthesis is more surprising in the case of $Sr_4Mn_2FeO_{9.80}$ than in that of the Ca analogue because $Sr_4Mn_3O_{10}$ is not[17] an $n = 3$ RP phase. The replacement of 33% of the Mn cations by Fe has thus stabilized this structure relative to a structure in which the transition metal cations occur in groups of three face-sharing octahedra, adjacent groups being linked by a common vertex. Our results are consistent with the prediction[17] that, for a given alkaline earth cation, the $n = 3$ structure increases in stability as the size of the transition metal cation increases. However, this simple size-based argument does not take into account the influence of the partial ordering of the Mn and Fe cations over the octahedral sites. We have previously argued that the distortion of the ideal tetragonal structure which occurs in the case of $Ca_4Mn_3O_{10}$ is necessary in order to accommodate the coordination requirements of the relatively small Ca^{2+} cation. The mixed Mn/Fe compound apparently achieves this by means of local disorder rather than by a cooperative distortion, that is, the presence of a disordered cation array on the B sites suppresses the ordered tilting of BO_6 octahedra which is favored by the A site. Although the volume/formula unit is ~2% larger in $Ca_4Mn_2FeO_{9.75}$ than in $Ca_4Mn_3O_{10}$, the radius of the 12-coordination shell around Ca(1) (in the perovskite blocks) is shorter in the former. Similarly, the 9-coordinate shell around Ca(2) (in the rock salt layers) is markedly (~0.18 Å) shorter than that in $Ca_4Mn_3O_{10}$. The decrease in size of the coordination sphere around Ca(1) may be due in part to the increased concentration of vacancies on the anion sublattice. If our refinements are reliable, this explanation does not extend to the environment of Ca(2), which includes neither O(1) nor O(4). The Mn/Fe(1) octahedra in $Ca_4Mn_2FeO_{9.75}$ are compressed along *z* and thus contrast with the regular octahedra found at the center of the perovskite blocks in $Ca_4Mn_3O_{10}$. The refinements suggest that the anion vacancies occur on those sites that coordinate the Fe-rich Mn/Fe(1) site, and this in turn suggests that the reduced Fe^{3+} cations preferentially occupy this site. Indeed, the fraction (0.576) of the Mn/Fe(1) sites occupied by Fe is such that all the Fe^{3+} cations could be accommodated here. The proposed vacancy distribution would be consistent with the observation of a mean Mn/Fe(1)−O bond length which is shorter than that observed in $Ca_4Mn_3O_{10}$, despite the fact that the site has been substituted with cations which are larger than the original Mn^{4+}. There is a greater spread in the average bond lengths around the Mn/Fe(2) site, with the bond to O(2) (in the rock salt layer) being significantly longer (1.935(7) Å) than the trans bond to O(1) (1.915(7) Å). The relative lengths of the axial bonds in this octahedron are thus reversed with respect to those observed in the corresponding octahedron in $Ca_4Mn_3O_{10}$ (1.891(5) and 1.921(6) Å, respectively). We explained the structure of the latter compound by arguing that Mn(1) and Mn(2) compete for the electron density on O(1), whereas there is little competition for the electron density on O(2), thus resulting in a short Mn(2)−O(2) bond and a longer Mn(2)−O(1) bond. In the case of $Ca_4Mn_2FeO_{9.75}$, we must

(15) Takeda, Y.; Kanno, K.; Takada, T.; Yamamoto, O.; Takano, M.; Nakayama, N.; Bando, Y. *J. Solid State Chem.* **1986**, *63*, 237.
(16) Battle, P. D.; Gibb, T. C. *J. Chem. Soc., Dalton Trans.* **1987**, 667.
(17) Rossell, H. J.; Goodman, P.; Bulcock, S.; March, R. H.; Kennedy, S. J.; White, T. J.; Lincoln, F. J.; Murray, K. S. *Aust. J. Chem.* **1996**, *49*, 205.

Table 2. Bond Lengths (Å) and Bond Angles (deg) in $Ca_4Mn_2FeO_{9.75}$ at Room Temperature[a]

Ca(1)−O(1)	2.6432(1)	4× (97%)	Ca(2)−O(2)	2.303(3)	1×
Ca(1)−O(3)	2.461(4)	4× (50%)		2.6509(2)	4×
	2.791(4)	4× (50%)	Ca(2)−O(3)	2.382(3)	4× (50%)
Ca(1)−O(4)	2.469(2)	4× (45%)		2.722(4)	4× (50%)
	2.946(3)	4× (45%)			
Mn/Fe(1)−O(1)	1.876(2)	2× (97%)	Mn/Fe(2)−O(1)	1.915(7)	1× (97%)
Mn/Fe(1)−O(4)	1.9002(5)	8× (45%)	Mn/Fe(2)−O(2)	1.935(7)	1×
			Mn/Fe(2)−O(3)	1.8828(5)	8× (50%)
Mn/Fe(1)−O(4)−Mn/Fe(1)	159.0(2)				
Mn/Fe(2)−O(3)−Mn/Fe(2)	165.8(2)				

[a] Mean Mn/Fe(1)−O: 1.892(10) Å, $(r_{ax} - r_{eq})/(r_{ax} + r_{eq}) = -0.0064$. Mean Mn/Fe(2)−O: 1.896(20) Å, $(r_{ax} - r_{eq})/(r_{ax} + r_{eq}) = 0.0110$.

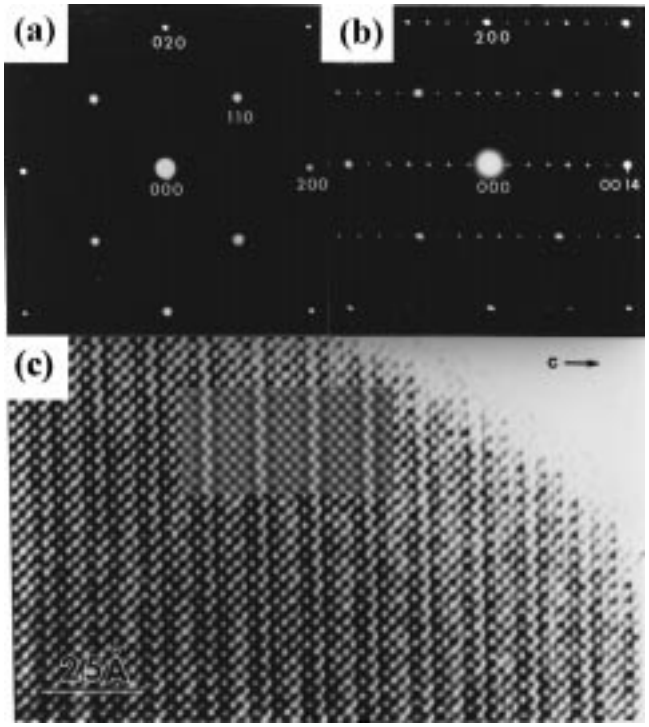

Figure 5. Electron diffraction patterns of $Ca_4Mn_2FeO_{9.75}$ taken along (a) [001] and (b) [010]. (c) Observed and simulated [010] lattice images of $Ca_4Mn_2FeO_{9.75}$.

argue that the presence of trivalent iron on the Mn/Fe(1) site weakens the competition for the electron density on O(1), hence strengthening the Mn/Fe(2)−O(1) bond at the expense of the Mn/Fe(2)−O(2) bond. The resulting distortion, with the longer bond directed into the rock salt layer, is similar to that observed in previous studies on $n = 2$ RP compounds[18] containing Jahn−Teller (JT) active Mn^{3+}. The differing extent of the distortions around the two Mn/Fe sites can be quantified with the parameter $(r_{ax} - r_{eq})/(r_{ax} + r_{eq})$ where $r_{ax(eq)}$ is the mean axial (equatorial) bond length in the octahedra. The values listed in Table 2 show the extent to which the Fe^{3+}-rich site is more regular than the Fe^{4+} site, which has an intrinsic lack of symmetry and is therefore more suited to the JT cation. The presence of Fe^{4+}: $t_{2g}^3\ e_g^1$ cations on the Mn/Fe(2) site is likely to lead to local structural strain because of JT distortions. This aperiodic strain, together with that created by the presence of a disordered cation array, may make it favorable for the O(3) sublattice in $Ca_4Mn_2FeO_{9.75}$ to undergo local displacive disorder in a tetragonal structure, rather than a concerted transition to orthorhombic symmetry, as occurs in $Ca_4Mn_3O_{10}$. This argument cannot be extended to account for the local displacement of O(4), which is coordinated to a cation site (Mn/Fe(1)) with a very small (5.7%) concentration of JT cations. We are led to assume that the displacements within the outer layers of the perovskite blocks dictate the structural chemistry of this compound. Consideration of the disordered distribution of sites (Figure 3) available to O(3) and O(4) suggests that, in the absence of the structural relaxation afforded by local perturbations, anion−anion repulsions, brought about by short contact distances, would ensure the selection of one of the two sets of sites (dotted and solid circles) and hence cause a cooperative phase transition. Such an ordering of the anion displacements, equivalent to a rotation of the octahedra about [001], has been observed in the $n = 1$ RP phase Sr_2IrO_4,[19] although the degree of order has been questioned.[20] The IrO_6 octahedra in the $n = 2$ phase $Sr_3Ir_2O_7$[21] are also rotated about [001], but there is no correlation between neighboring bilayers of octahedra and possibly none between the two perovskite sheets in any one bilayer. In view of the absence of anion displacements, ordered or otherwise, in $Sr_3Ti_2O_7$,[22] it was suggested[21] that the degree of rotation is determined by electronic factors, rather than by cation size. However, the fact that $Sr_3Ru_2O_7$ has an ideal $n = 2$ RP structure[23] suggests that the problem is too complex to be accounted for by any single variable. The absence of disorder in the z parameters of the anions in the present case shows that the latent distortion in $Ca_4Mn_2FeO_{9.75}$ resembles that seen in $n = 1$ Ca_2MnO_4[24] more closely than that observed in $n = 3$ $Ca_4Mn_3O_{10}$;[8] it also shows that the relatively poor crystallinity of the sample along [001] does not derive from atomic disorder. The resistivity data described above show that the 3d valence electrons are localized in this compound. This is due in part to the relatively narrow energy width of the 3d bands, but delocalization will also be inhibited by the structural disorder present.

The structure of $Sr_4Mn_2FeO_{9.80}$ differs from that of the Ca analogue in a number of ways. Perhaps most obviously, the structure is able to retain tetragonal

(18) Battle, P. D.; Millburn, J. E.; Rosseinsky, M. J.; Spring, L. E.; Vente, J. F.; Radaelli, P. G. *Chem. Mater.* **1997**, *9*, 3136.

(19) Crawford, M. K.; Subramanian, M. A.; Harlow, R. L.; Fernandez-Baca, J. A.; Wang, Z. R.; Johnson, D. C. *Phys. Rev.* **1994**, *B49*, 9198.

(20) Huang, Q.; Soubeyroux, L.; Chmaissem, O.; Natali-Sora, I.; Santoro, A.; Cava, R. J.; Krajewski, J. J.; Peck, W. F., Jr. *J. Solid State Chem.* **1994**, *112*, 355.

(21) Subramanian, M. A.; Crawford, M. K.; Harlow, R. L. *Mater. Res. Bull.* **1994**, *29*, 645.

(22) Elcombe, M. M.; Kisi, E. H.; Hawkins, K. D.; White, T. J.; Goodman, P.; Matheson, S. *Acta Crystallogr.* **1991**, *B47*, 305.

(23) Müller-Buschbaum, H.; Wilkens, J. *Z. Anorg. Allg. Chem.* **1990**, *591*, 161.

(24) Leonowicz, M. E.; Poppelmeier, K. R.; Longo, J. M. *J. Solid State Chem.* **1985**, *59*, 71.

Table 3. Structural Parameters of $Sr_4Mn_2FeO_{9.80}$ at Room Temperature[a]

atom	site	fractional occupancy	*x*	*y*	*z*	U_{iso}, U_{eq} (Å^2)	U_{11} (Å^2)	U_{22} (Å^2)	U_{33} (Å^2)
Sr(1)	4e	1	0	0	0.56992(6)	0.0082(4)			
Sr(2)	4e	1	0	0	0.70162(6)	0.0049(4)			
Mn/Fe(1)	2a	0.548/0.452(4)	0	0	0	0.010(2)			
Mn/Fe(2)	4e	0.726/0.274(2)	0	0	0.1400(3)	0.012(2)			
O(1)	4e	0.94(1)	0	0	0.0682(1)	0.0091	0.007(2)	0.007(2)	0.012(2)
O(2)	4e	1	0	0	0.20898(8)	0.0071	0.010(1)	0.010(1)	0.002(1)
O(3)	8g	1	0	0.5	0.63772(5)	0.0075	0.007(1)	0.003(1)	0.014(1)
O(4)	4c	0.96(1)	0	0.5	0.5	0.0175	0.013(2)	0.022(2)	0.018(2)

[a] Space group *I*4/*mmm*; $a = 3.83393(1)$ Å, $c = 27.8148(1)$ Å, $V = 408.851(3)$ Å^3. For all O, $U_{12} = U_{13} = U_{23} = 0$. Agreement indices: neutrons, $R_{wp} = 5.12\%$, $R_p = 4.48\%$, DWd = 0.86; X-rays, $R_{wp} = 7.57\%$, $R_p = 5.96\%$, DWd = 1.74; totals, $R_{wp} = 5.84\%$, $R_p = 5.87\%$, DWd = 1.23. $\chi_{red}^2 = 1.64$ for 52 variables.

Table 4. Bond Lengths (Å) and Bond Angles (deg) in $Sr_4Mn_2FeO_{9.80}$ at Room Temperature[a]

Sr(1)−O(1)	2.71142(5)	4× (94%)	Sr(2)−O(2)	2.488(2)	1×
Sr(1)−O(3)	2.689(2)	4×		2.7188(2)	4×
Sr(1)−O(4)	2.730(1)	4× (96%)	Sr(2)−O(3)	2.614(2)	4×
Mn/Fe(1)−O(1)	1.896(2)	2× (94%)	Mn/Fe(2)−O(1)	1.997(8)	1× (94%)
Mn/Fe(1)−O(4)	1.91697(1)	4× (96%)	Mn/Fe(2)−O(2)	1.919(8)	1×
			Mn/Fe(2)−O(3)	1.9180(3)	4×
Mn/Fe(1)−O(4)−Mn/Fe(1)	180.0(0)				
Mn/Fe(2)−O(3)−Mn/Fe(2)	176.0(4)				

[a] Mean Mn/Fe(1)−O: 1.909(9) Å, $(r_{ax} - r_{eq})/(r_{ax} + r_{eq}) = -0.0055$. Mean Mn/Fe(2)−O: 1.931(29) Å, $(r_{ax} - r_{eq})/(r_{ax} + r_{eq}) = 0.0103$.

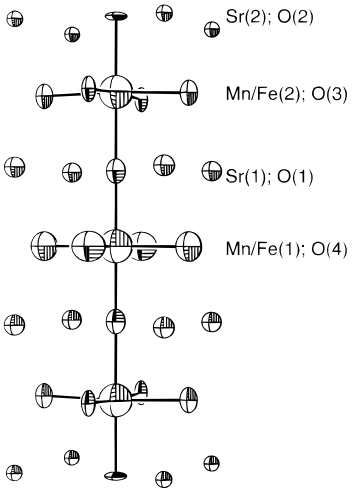

Figure 6. Anisotropic displacement ellipsoids (95%) in $Sr_4Mn_2FeO_{9.80}$

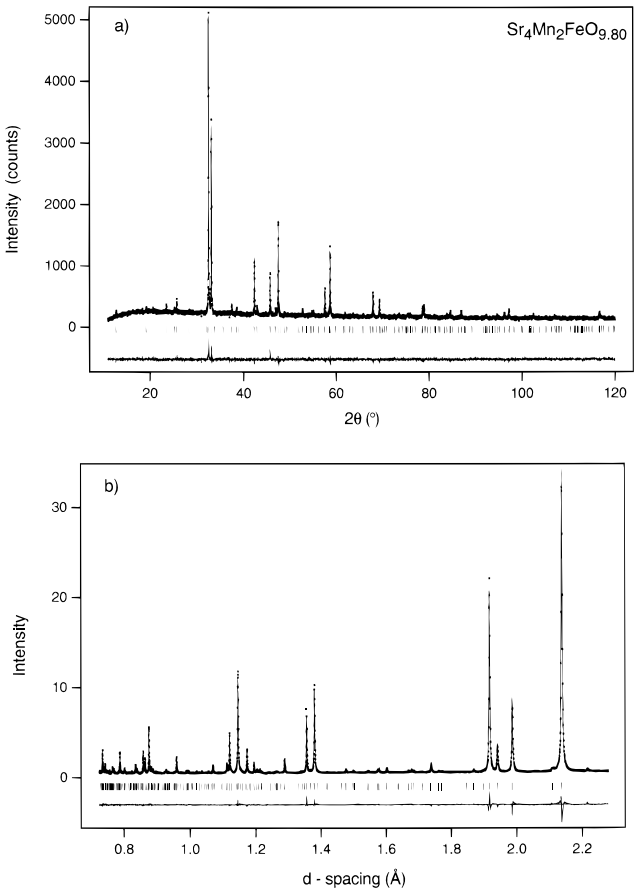

Figure 7. Observed, calculated, and difference (a) X-ray and (b) neutron diffraction profiles of $Sr_4Mn_2FeO_{9.80}$ at room temperature. Reflection positions are marked.

symmetry without the introduction of disorder onto the anion sublattice. Presumably, the coordination requirements of the Sr cation are more readily met in a unit cell which is 8% larger than that of the Ca compound. This expansion is isotropic, with the consequence that the Mn/Fe(1,2)−O(3,4) bonds in the *xy* plane are longer in the Sr compound. A more dramatic change occurs in the lengths of the bonds which lie along *z*, namely, that Mn/Fe(2)−O(2) < Mn/Fe(2)−O(1), as was the case in $Ca_4Mn_3O_{10}$. To rationalize this change, we could argue that, assuming all Fe^{3+} cations are found at the center of the perovskite blocks, the concentration of tetravalent cations, both Mn^{4+} and Fe^{4+}, on site Mn/Fe(1) has increased from 50% to 60% on moving from the Ca to the Sr compound. This will increase the competition for the electron density on O(1) and hence will act to lengthen the Mn/Fe(2)−O(1) bond relative to the Mn/Fe(2)−O(2) bond; the latter bond is shorter in $Sr_4Mn_2FeO_{9.80}$ than in $Ca_4Mn_2FeO_{9.75}$, despite the expansion of the unit cell. However, the magnitude of these changes is remarkable, and we doubt whether the above explanation is adequate. It may also be significant that a larger fraction (27.4(2)%) of the Mn/Fe(2) sites are occupied by Fe^{4+} in $Sr_4Mn_2FeO_{9.80}$ than in $Ca_4Mn_2FeO_{9.75}$ (21.2(2)%), and it is also possible that the change in the local environment can be attributed to the establishment of a cooperative Jahn−Teller distortion. This would be consistent with the absence of static disorder on the O(3) sublattice in $Sr_4Mn_2FeO_{9.80}$, which we have previously argued was necessary to accom-

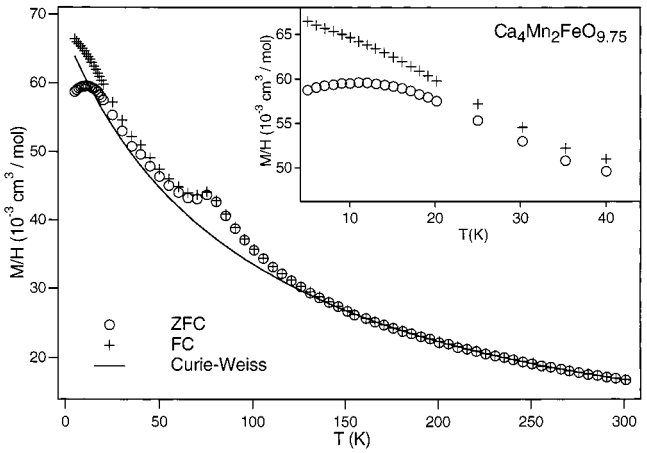

Figure 8. Temperature dependence of the FC and ZFC molar magnetic susceptibility of $Ca_4Mn_2FeO_{9.75}$, measured at 100 G.

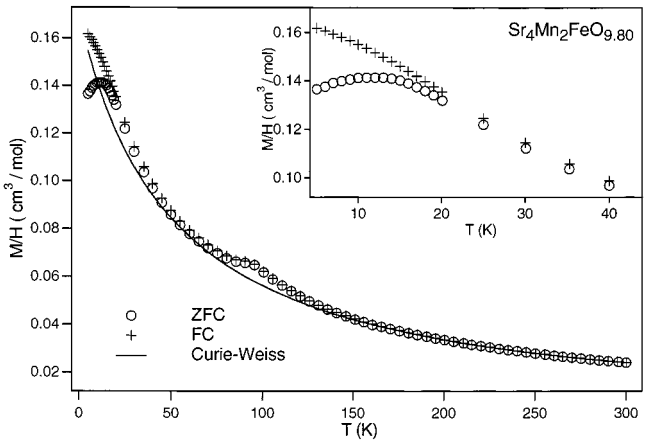

Figure 9. Temperature dependence of the FC and ZFC molar magnetic susceptibility of $Sr_4Mn_2FeO_{9.80}$, measured at 100 G.

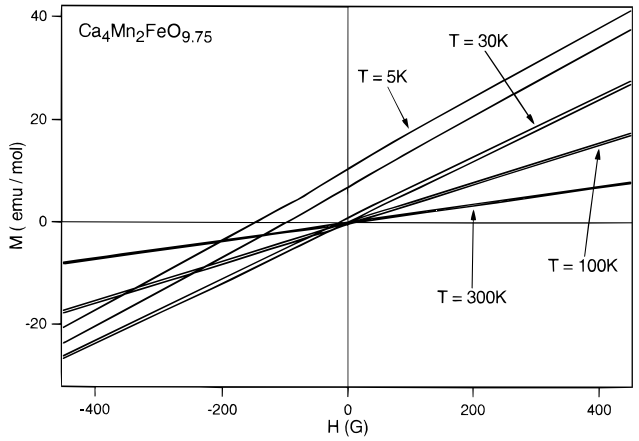

Figure 10. Central region of $M(H)$ as a function of temperature for $Ca_4Mn_2FeO_{9.75}$

Table 5. Magnetic Properties of $Ca_4Mn_2FeO_{9.75}$ and $Sr_4Mn_2FeO_{9.80}$

	T_g (K)	T_N (K)	θ (K)	C_m (cm^3 K mol^{-1})
$Ca_4Mn_2FeO_{9.75}$	11	75	−99(1)	6.71(3)
$Sr_4Mn_2FeO_{9.80}$	12	90	−49(1)	8.38(3)

modate local, noncooperative Jahn−Teller distortions. It would also be consistent with the bond length asymmetry being much greater in the present case than in $Ca_4Mn_3O_{10}$. Anion disorder made a detailed interpretation of the thermal parameters of $Ca_4Mn_2FeO_{9.75}$ difficult, but Figure 6 shows enhanced displacements at the O(4) site in $Sr_4Mn_2FeO_{9.80}$ compared to the other partially occupied site, O(1); this may reflect the lower degree of Mn/Fe disorder at site Mn/Fe(2), to which O(1), but not O(4), is adjacent. The anion site with the smallest thermal ellipsoid is O(2) in the rock salt layer, indicating a relatively high degree of order around this site. This is also the only ellipsoid which is significantly elongated in the *xy* plane. The large isotropic temperature factors of the Mn/Fe sites reflect the cation disorder on these sites and also the low mean scattering length, and hence poor definition, of the site in the neutron experiment.

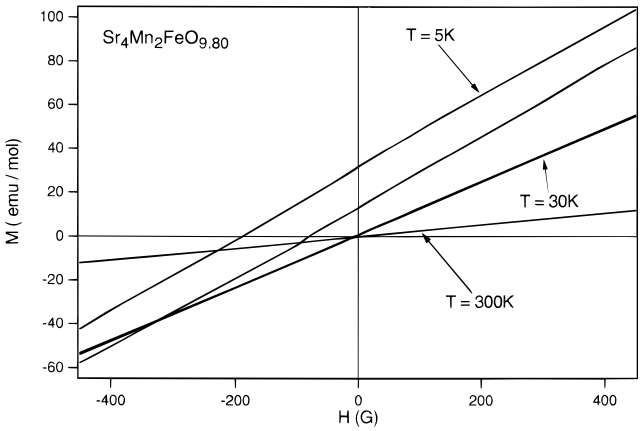

Figure 11. Central region of $M(H)$ as a function of temperature for $Sr_4Mn_2FeO_{9.80}$

The magnetic susceptibilities of $Ca_4Mn_2FeO_{9.75}$ and $Sr_4Mn_2FeO_{9.80}$ are qualitatively very similar (Figures 8 and 9). The negative values of the Weiss constant (θ, Table 5) indicate that antiferromagnetic interactions dominate in both compounds. The higher Néel temperature of the latter can be understood if we assume that the more electropositive Sr^{2+} cation competes less effectively than Ca^{2+} for the negative charge density on the oxide ions, thus leaving this charge available for covalent interaction with the transition metal cations, and hence strengthening the magnetic superexchange interactions. However, the present case is perhaps too complex to allow the use of this simple argument which ignores the difference in the nature of the oxide sublattices in the two compounds. This is perhaps indicated by the fact that the compound with the more negative value of θ actually has the lower T_N. We shall discuss the magnetic properties of $Ca_4Mn_2FeO_{9.75}$ in detail, and in view of the similar susceptibility behavior, we would normally expect the same arguments to apply to the Sr analogue. However, the different degrees of disorder on the anion sublattice may reduce the validity of this extrapolation, and the inversion of the bond asymmetry around Mn/Fe(2) may also prove to introduce significant magnetic differences. A low-temperature study of $Sr_4Mn_2FeO_{9.80}$ by neutron diffraction is needed to test the validity of the analogy. In the case of $Ca_4Mn_2FeO_{9.75}$, our neutron data clearly demonstrate that the compound shows long-range magnetic order below 75 K, allowing the identification of the maximum in χ with T_N. However, the Mn/Fe(1) site at the center of the perovskite blocks, where the cation disorder is greater, does not appear to participate in the ordering, and the ordered component of the magnetic moment at the Mn/

Table 6. Structural Parameters of $Ca_4Mn_2FeO_{9.75}$ at 5 K[a]

atom	site	fractional occupancy	x	y	z	U_{iso}, U_{eq} (Å^2)	U_{11} (Å^2)	U_{22} (Å^2)	U_{33} (Å^2)
Ca(1)	4e	1	0	0	0.5711(2)	0.009(1)			
Ca(2)	4e	1	0	0	0.7039(2)	0.004(1)			
Mn/Fe(1)	2a	0.424/0.576	0	0	0	0.003(2)[b]			
Mn/Fe(2)	4e	0.782/0.212	0	0	0.1394(2)[c]	0.003(2)[b]			
O(1)	4e	0.97	0	0	0.0693(2)	0.030	0.044(3)	0.044(3)	0.002(3)
O(2)	4e	1	0	0	0.2111(2)	0.010	0.017(1)	0.017(1)	−0.004(3)
O(3)	16n	0.5	0	0.561(1)	0.6394(2)[c]	0.008	0.006(2)	−0.006(6)	0.025(2)
O(4)	8j	0.452	0	0.595(2)	$^1/_2$	0.0190	−0.004(4)	0.009(7)	0.053(5)

[a] Space group $I4/mmm$; $a = 3.72964(2)$ Å, $c = 27.0376(3)$ Å, $V = 376.099(5)$ Å^3. For all O, $U_{12} = U_{13} = U_{23} = 0$, except for O(3), where $U_{12} = U_{13} = 0$, $U_{23} = -0.005(1)$ Å^2. Agreement indices: $R_{wp} = 3.28\%$, $R_p = 2.62\%$, DWd = 1.03; $\chi_{red}^2 = 1.85$ for 36 variables. [b] Constrained to be equal. [c] Constrained to differ by 0.5.

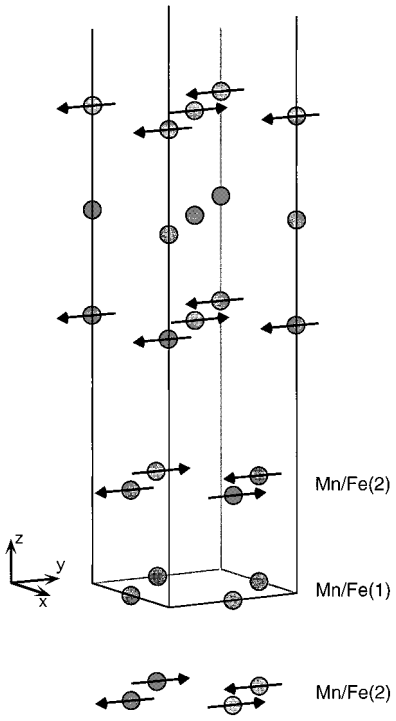

Figure 12. Antiferromagnetic structure of $Ca_4Mn_2FeO_{9.75}$ drawn in the magnetic unit cell. Only Mn/Fe cations are shown.

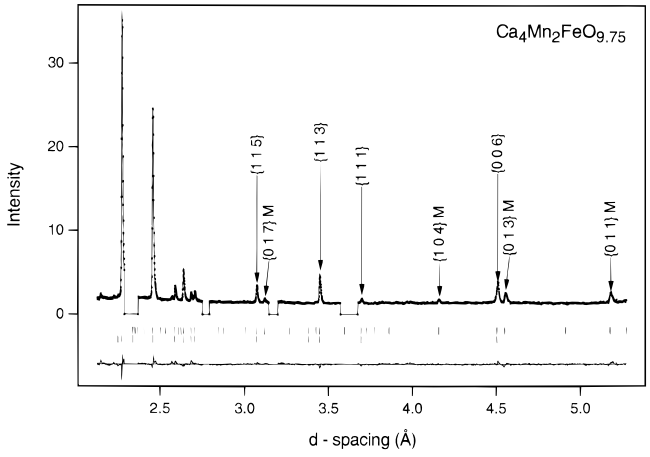

Figure 13. Observed, calculated, and difference neutron diffraction profiles (IRIS) of $Ca_4Mn_2FeO_{9.75}$ at 5 K. Reflection positions, indexed in the magnetic unit cell, are marked; regions containing scattering from the cryostat have been excluded.

Fe(2) site is reduced to such an extent that we conclude that some cations on the edges of the blocks may remain magnetically disordered below T_N. These decoupled

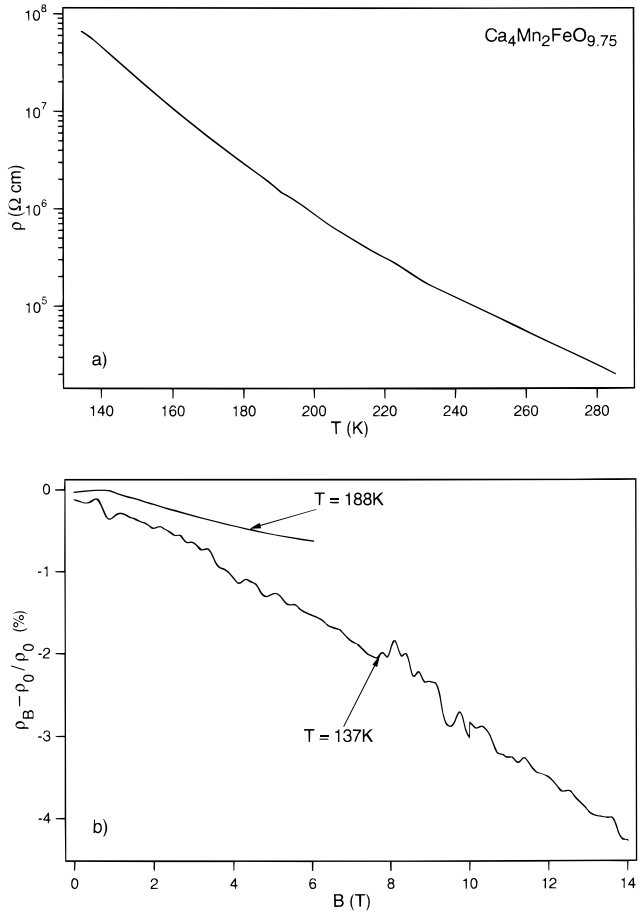

Figure 14. (a) Resistivity of $Ca_4Mn_2FeO_{9.75}$ as a function of temperature (b) Magnetoresistance of $Ca_4Mn_2FeO_{9.75}$ as a function of magnetic field at 137 and 188 K.

spins freeze in a spin glass transition at ∼11 K, consistent with the observation of displaced, finite-width $M(H)$ hysteresis loops at 5 K, but not at temperatures of 30 K and above. The absence of observable long-range magnetic order in the central layer suggests that a considerable degree of magnetic frustration is present. The presence of displaced and partially occupied anion sites will perturb the magnetic superexchange interactions, but the absence of order can also be explained in terms of the competing interactions between the $3d^3$ Mn^{4+}, $3d^4$ Fe^{4+}, and $3d^5$ Fe^{3+} cations which are present. The interaction between nearest neighbor (NN) Mn^{4+}/Mn^{4+} or Fe^{3+}/Fe^{3+} cation pairs will be unambiguously antiferromagnetic, but that between NN Mn^{4+} and Fe^{3+} cations will be antiferromagnetic through the π orbitals and ferromagnetic through the σ orbitals. This can lead to spin glass formation, as is evidenced by the fact that

none of the RP phases Sr_2FeRuO_6 ($n = \infty$), Sr_4FeRuO_8 ($n = 1$), and Sr_3FeRuO_7 ($n = 2$), which contain a disordered array of $3d^5$ Fe^{3+} and $4d^3$ Ru^{5+}, shows long-range magnetic order but all behave as spin glasses at low temperatures (<30 K),[25,26] despite the fact that the lattice is not geometrically frustrated. In the present case, the presence of Fe^{4+} introduces further complexities because the σ superexchange between a pair of Fe^{4+} cations may be ferromagnetic or antiferromagnetic depending on the local disposition of the oxide ions. We have previously discussed[27] how interactions between d^4 and d^3 cations can lead to spin glass formation in the insulating $n = 2$ RP phase $Sr_2NdMn_2O_7$. It is thus unsurprising that long-range magnetic order is not established on the Mn/Fe(1) sublattice. The majority of these arguments are also valid when discussing the Mn/Fe(2) sublattice, where the degree of cation disorder is lower. Although Fe^{3+} cations are expected to be absent from this site, the cations in the outer layer will obviously interact with those in the central layer. However, it appears that the frustration is reduced sufficiently to allow a small ordered magnetic moment to be established at the former sites. We cannot tell from our neutron data whether all the sites order with a low moment or whether a smaller number of sites order with a relatively large moment; Mössbauer spectroscopy may resolve this issue in the future. The fact that the magnetic ordering is 3D, that is there is a well-defined relationship between the spin directions in the two layers which border each block, suggests that the cations in the central layer must be involved in the magnetic ordering. It is possible that they do carry an ordered moment but that it is too small to be detected in the experiments described above. These arguments describe possible influences on the magnetic ordering within an $n = 3$ block. However, it is important to remember that there is also a correlation between the ordered spins in neighboring blocks. In the absence of local strain, the tetragonal symmetry of the $Ca_4Mn_2FeO_{9.75}$ structure would leave these interactions frustrated, and this frustration may be as important as the competing intrablock interactions in reducing the ordered magnetic moment. The orthorhombic distortion in $Ca_4Mn_3O_{10}$ eliminates this frustration in the undoped compound. It is interesting to note that although the magnetic moment in $Ca_4Mn_2FeO_{9.75}$ is much lower than that observed in $Ca_4Mn_3O_{10}$, the reduction in the Néel temperature, from 115 to 75 K, is less drastic. The retention of tetragonal symmetry by $Ca_4Mn_2FeO_{9.75}$ also excludes the possibility of a weak ferromagnetic state forming at low temperatures via the DM mechanism, and this may explain why the magnetoresistance of the Fe-doped phase is less than that of the parent compound.[9]

In conclusion, we have demonstrated that 33% of the transition metal sites in $Ca_4Mn_3O_{10}$ can be substituted by Fe and that the same doping level is enough to convert the Sr analogue to the $n = 3$ RP structure; both Fe-doped compounds are oxygen deficient. Spin glass behavior and the reduction in the staggered moment indicate that the initial aim of introducing competing d^3-d^4 ferromagnetic coupling by Fe(IV) substitution was successfully achieved, but electron localization makes these super-exchange rather than double-exchange interactions, accounting for the absence of large magnetoresistance. Neither compound shows the CMR that we had hoped to observe, but both illustrate the complexities of structural solid-state chemistry and the extent to which the electronic properties of an oxide are controlled by the crystal structure.

Acknowledgment. We are grateful to EPSRC for financial support.

CM9807384

(25) Battle, P. D.; Bollen, S. K.; Powell, A. V. *J. Solid State Chem.* **1992**, *99*, 267.
(26) Battle, P. D.; Gibb, T. C.; Jones, C. W.; Studer, F. *J. Solid State Chem.* **1989**, *78*, 281.
(27) Battle, P. D.; Green, M. A.; Laskey, N. S.; Millburn, J. E.; Radaelli, P. G.; Rosseinsky, M. J.; Sullivan, S. P.; Vente, J. F. *Phys. Rev. B* **1996**, *54*, 15967.